JACS
JOURNAL OF THE AMERICAN CHEMICAL SOCIETY
Article
pubs.acs.org/JACS

In Vivo Multimodality Imaging and Cancer Therapy by Near-Infrared Light-Triggered *trans*-Platinum Pro-Drug-Conjugated Upconverison Nanoparticles

Yunlu Dai,[†,∥] Haihua Xiao,[⊥] Jianhua Liu,[§] Qinghai Yuan,[§] Ping'an Ma,[†,*] Dongmei Yang,[†] Chunxia Li,[†] Ziyong Cheng,[†] Zhiyao Hou,[†] Piaoping Yang,[‡,*] and Jun Lin[†,*]

[†]State Key Laboratory of Rare Earth Resource Utilization, Changchun Institute of Applied Chemistry, Chinese Academy of Sciences, Changchun, 130022, People's Republic of China

[‡]Key Laboratory of Superlight Materials and Surface Technology, Ministry of Education, Harbin Engineering University, Harbin, 150001, People's Republic of China

[§]Department of Radiology, The Second Hospital of Jilin University, Changchun, 130022, People's Republic of China

[⊥]Department of Chemical and Biomolecular Engineering, University of Notre Dame, Notre Dame, Indiana 46556, United States

[∥]University of Chinese Academy of Sciences, Beijing 100049, People's Republic of China

Supporting Information

ABSTRACT: Controlling anticancer drug activity and release on demand is very significant in cancer therapy. The photoactivated platinum(IV) pro-drug is stable in the dark and can be activated by UV light. In this study, we develop a multifunctional drug delivery system combining upconversion luminescence/magnetic resonance/computer tomography tri-modality imaging and NIR-activated platinum pro-drug delivery. We use the core−shell structured upconversion nanoparticles to convert the absorbed NIR light into UV to activate the *trans*-platinum(IV) pro-drug, *trans,trans,trans*-$[Pt(N_3)_2(NH_3)(py)(O_2CCH_2CH_2COOH)_2]$. Compared with using the UV directly, the NIR has a higher tissue penetration depth and is less harmful to health. Meanwhile, the upconversion nanoparticles can effectively deliver the platinum(IV) pro-drugs into the cells by endocytosis. The mice treated with pro-drug-conjugated nanoparticles under near-infrared (NIR) irradiation demonstrated better inhibition of tumor growth than that under direct UV irradiation. This multifunctional nanocomposite could be used as multimodality bioimaging contrast agents and transducers by converting NIR light into UV for control of drug activity in practical cancer therapy.

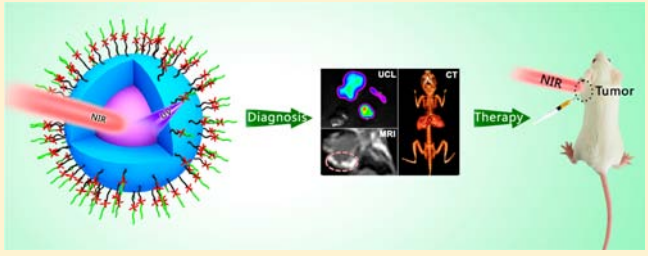

INTRODUCTION

A multifunctional hybrid system which combines two or more cancer diagnosis and therapy manners together to form nanomedical platforms has gained more and more attention.[1] Several different imaging techniques have been developed to monitor the physiological procedures in diagnostic medicine, such as computer tomography (CT), magnetic resonance imaging (MRI), ultrasound imaging, positron emission tomography (PET), and optical imaging.[2] However, the single-modality imaging cannot meet the higher diagnosis requirement. For example, CT has high temporal resolution, but it is still difficult to distinguish subtle changes of soft tissues.[3] MRI provides an excellent spatial resolution but suffers from limited sensitivity.[4] Therefore, taking advantage of different modality imaging together, multimodal imaging can satisfy the medical research and diagnosis. Lanthanide-doped upconversion nanoparticles have attracted a tremendous amount of attention in recent years due to their upconversion luminescent properties.[5] Compared with other optical imaging technology, upconversion luminescence (UCL) converts the low-energy photons (NIR) into high-energy photons (UV, visible, or NIR) via the multiphoton processes. Meanwhile, UCL exhibits unique properties, such as large Stokes shift, sharp emission lines, and superior photostability.[6] Especially, Tm^{3+}-doped UCNPs can emit 800 nm NIR light under 980 nm laser excitation (NIR-to-NIR), which can be used as an optical probe for deep tissue imaging due to the high tissue penetration depth of NIR.[2c] In addition, Gd-based/doped upconversion nanoparticles can be used as contrast agents for MRI due to their unpaired 4f electrons.[7] Yb- and Gd-based/doped upconversion nanoparticles have been developed as excellent CT contrast agents because of their high atomic and strong X-ray attenuation.[3] Hence, the development of multimodal imaging in one system is of great interest for cancer diagnosis.

Received: September 30, 2013
Published: November 26, 2013

   dx.doi.org/10.1021/ja410028q | *J. Am. Chem. Soc.* 2013, 135, 18920−18929

After diagnosis through upconversion nanoparticle-based multimodality imaging technology, cancer therapy is the final goal. Chemotherapy has been used for several decades to treat cancer.[8] Among all the anticancer drugs, cisplatin is widely applied to treat various types of cancer. However, their application is limited due to toxic side effects and drug resistance.[9] The toxicity of light-activated platinum(IV) pro-drugs can be controlled, thereby avoiding damage to normal tissue.[10] Sadler's group has reported that *trans*-platinum(IV) complexes *trans,trans,trans*-$[Pt(N_3)_2(NH_3)(py)(OH)_2]$ and *trans,trans,trans*-$[Pt(N_3)_2(py)_2(OH)_2]$ can also be activated to higher toxic platinum(II) complexes by UV, blue, and green light via an unusual mechanism of action, which differs from the *cis* complexes.[11] However, the short wavelength lights (UV or visible light) have limited application in vivo due to damage to normal tissue and poor penetration into tissue.[12] To solve these problems, Yb/Tm-codoped upconversion nanoparticles can be used as an effective UV source by multiphoton absorption of NIR light, which has the deepest tissue penetration and is safe to the biological specimen.[13] For example, Zhang and co-workers have reported that UCNPs can be used for activating photocaged nucleic acids by absorbing NIR light and emitting UV light via upconversion nanoparticles.[13b] Shi's group have modified an azobenzene group into the mesoporous silica-coated upconversion nanoparticles to control the drug release by NIR light.[13f] Despite numerous efforts in this field, there is no report on the use of UCNPs as the carriers to deliver light-activated pro-drug through NIR-to-UV strategy together with trimodality imaging (UCL/MR/CT imaging).

Herein, we demonstrate a multifunctional drug delivery system which combines UCL/MR/CT trimodality imaging and NIR-activated platinum pro-drug delivery together. The core–shell structured upconversion nanoparticles $NaYF_4:Yb^{3+}/Tm^{3+}@NaGdF_4/Yb^{3+}$ (denoted as UCNPs) are used as the drug carriers. Meanwhile, the UCNPs can be used for in vivo UCL, MR, and CT imaging. Furthermore, the dicarboxyl light-activated platinum(IV) pro-drugs *trans,trans,trans*-$[Pt(N_3)_2(NH_3)(py)(O_2CCH_2CH_2COOH)_2]$ (denoted as DPP) have been conjugated on the surface of UCNPs. Finally, we coated UCNP-DPP with a monolayer of PEG. The aim of this study is to combine cancer diagnosis and therapy together to achieve the following goals: (1) the core–shell structured UCNPs were used for both in vitro and in vivo NIR-to-NIR UCL and T_1-weighted MR and CT imaging; (2) the *trans*-platinum(IV) pro-drug DPP can be activated to higher toxic platinum(II) complexes via the NIR-to-UV strategy, and in vivo tumor growth inhibition efficacies of UCNP-DPP-PEG under NIR irradiation were studied in detail.

EXPERIMENTAL SECTION

Synthesis of Oleic-Acid-Stabilized β-$NaYF_4:Yb^{3+}/Tm^{3+}$. Oleic-acid-capped β-$NaYF_4:Yb^{3+}/Tm^{3+}$ was synthesized according to the method developed previously.[14] In a typical procedure of preparing β-$NaYF_4:Yb^{3+}/Tm^{3+}$, 1 mmol of RE(oleate)$_3$ (RE = 59.5% Y + 40% Yb + 0.5% Tm), 12 mmol of NaF, and 20 mL of oleic acid (OA)/1-octadecene (ODE) (v/v = 1:1) mixed solvent were added to the reaction vessel and heated to 110 °C under a vacuum for 30 min to remove residual water and oxygen. After that, the temperature was increased to 320 °C and kept for 1.5 h in N_2 atmosphere environment. The β-$NaYF_4:Yb^{3+}/Tm^{3+}$ nanoparticles were obtained.

Synthesis of Oleic-Acid-Stabilized Core–Shell Structured $NaYF_4:Yb^{3+}/Tm^{3+}@NaGdF_4:Yb^{3+}$ Nanoparticles (UCNPs). First, the above-mentioned experiment was carried out. The cyclohexane solution of above was added to a four-neck reaction vessel. Ten milliliters of OA and 10 mL of ODE were added to the vessel, and the solvent was heated to 120 °C under a vacuum with magnetic stirring for 1 h and flushed with N_2. Then, the temperature was heated to 310 °C. Another bottle with 3 mL of OA/ODE (v/v = 1.5:1.5), Gd(CFCOO)$_3$ (0.98 mmol), Yb(CFCOO)$_3$ (0.02 mmol), and CFCOONa (1 mmol) was injected into the solution immediately. The reaction was kept at 310 °C for 1 h in N_2 atmosphere. The UCNPs were isolated by centrifugation. The core–shell structured nanoparticles were dispersed in chloroform for further use.

Preparation of PEI-Stabilized UCNPs. PEI (1.5 g) was dissolved in H_2O, and then the above UCNP chloroform solution was added followed by vigorously stirring for 24 h. The nanoparticles were separated by centrifugation and washed with deionized water to gain PEI-stabilized UCNPs.

Preparation of DPP-Conjugated UCNPs. PEI-UCNPs (100 mg) were dispersed in H_2O (20 mL). Ten milligrams of 1-(3-dimethylaminopropyl)-3-ethylcarbodiimide hydrochloride (EDC), 3 mg of *N*-hydroxysuccinimide (NHS), and 10 mg of DPP were added into the above solution and stirred overnight. The precipitates were separated by centrifugation and washed several times with deionized water.

Preparation of PEG-Modified UCNP-DPP Nanoparticles. mPEG-NH_2 (50 mg) was dissolved in H_2O (15 mL). EDC (8 mg) and NHS (2 mg) were added into the above solution and stirred at room temperature. Then, the UCNP-DPP was added to the above solution. After being stirred at room temperature for 6 h, the precipitates of UCNP-DPP-PEG were separated by centrifugation and washed several times with deionized water.

In Vitro Cytotoxicity of UCNP-DPP-PEG Nanoparticles. In vitro cytotoxicity of UCNP-DPP-PEG nanoparticles was assayed against HeLa cancer cells. HeLa cells were seeded in a 96-well plate with a density of 6000 cells per well and cultured in 5% CO_2 at 37 °C for 24 h. HeLa cells were then treated with UCNP-DPP-PEG for about 4 h, then irradiated with a 980 nm laser for 40 min (4.5 W/cm^2, 5 min break after 5 min irradiation). As the control, the HeLa cells treated with UCNP-DPP-PEG were left under UV for 40 min, and the HeLa cells only treated with UCNP-DPP-PEG were left in the dark. Then the cells were incubated for another 48 h in the dark. The concentrations of platinum were 3.75, 7.5, and 15 μM. At the end of the incubation, cells were then treated with 3-[4,5-dimethylthiazol-2-yl]-2,5-diphenyltetrazolium bromide (MTT) solution (diluted in a culture medium with a final concentration of 5 mg/mL) and incubated for another 4 h. Then the supernatant was removed, and 150 μL of DMSO was added to each well before the plate was examined using a microplate reader at the wavelength of 490 nm.

Upconversion Luminescence Microscopy (UCLM) Observation of the UCNP-DPP-PEG Nanoparticles. The instrument of UCLM was rebuilt on an inverted fluorescence microscope (Nikon Ti–S), and an external CW 980 nm diode laser was illuminated onto the samples. HeLa cells (5×10^4/well) were seeded in 6-well culture plates and grown overnight as a monolayer and were incubated with UCNP-DPP-PEG at 37 °C for different times. Then, the cells were washed with PBS three times, fixed with 2.5% formaldehyde (1 mL/well) at 37 °C for 10 min, and washed with PBS three times.

Cellular Uptake of the UCNP-DPP-PEG Nanoparticles. Cellular uptake was examined using ICP-MS. HeLa cells (1×10^5) were seeded in 6-well plates. These cells were then treated with UCNP-DPP-PEG nanoparticles (500 μg), and then incubated at 37 °C for 10 min, 30 min, 1 h, and 6 h. After being rinsed with PBS three times, the cells were lysed by cell lysis buffer. ICP-MS was used to determine the gadolinium contents in the cell lysis solution.

Laser Irradiation. A 980 nm NIR laser (BWT Beijing Ltd.) was used for irradiation of solution, cells, and mice. The power density of the NIR laser was fixed by fixing the power of the laser beam and the distance between the laser beam and the cells. The power density of the 980 nm NIR laser beam was determined by a power meter (Beijing Wuke LP-3).

Animal Experiments. Female Balb/c mice (18–20 g) were purchased from Center for Experimental Animals, Jilin University (Changchun, China). In vivo study conforms to the guidelines of The National Regulation of China for Care and Use of Laboratory Animals.

dx.doi.org/10.1021/ja410028q | J. Am. Chem. Soc. 2013, 135, 18920–18929

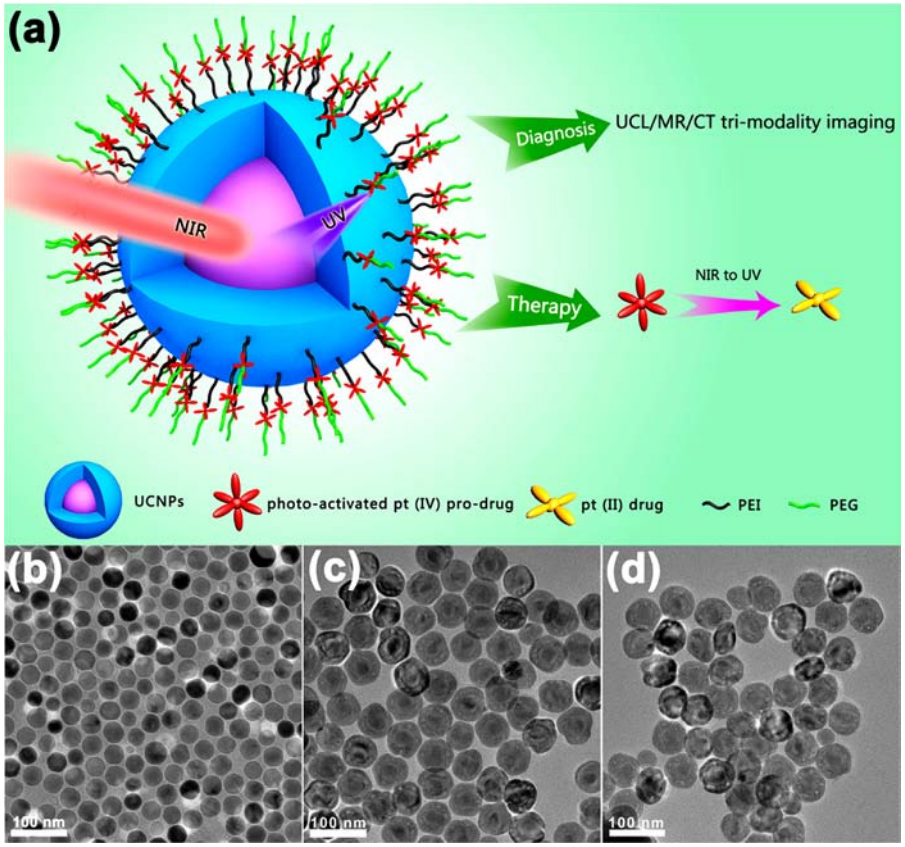

Figure 1. Schematic illustration of the characterization of UCNP-DPP-PEG nanoparticles (a). TEM images of oleic-acid-capped $NaYF_4:Yb^{3+}/Tm^{3+}$ nanoparticles (b), core−shell structured $NaYF_4:Yb^{3+}/Tm^{3+}@NaGdF_4:Yb^{3+}$ nanoparticles (c), and UCNP-DPP-PEG nanoparticles (d).

The tumors were established by subcutaneous injection of H22 cells (murine hepatocarcinoma cell lines) in the left axilla of each mouse. The tumors were allowed to grow for around 4 days to reach the size of around 100−200 mm^3.

In Vivo Toxicity Studies. The tumor-bearing mice were randomized into five groups (n = 6, each group) and were treated by intratumoral injection with UCNP-DPP-PEG and saline under different conditions. The injected Pt (conjugated nanoparticles) dose in 80 μL of saline was 0.65 mg/kg body weight. We injected the UCNP-DPP-PEG in the first three groups. After 4 h, we irradiated the tumor site with 980 nm laser for 30 min (2.5 W/cm^{-2}, 5 min break after 5 min irradiation, group 1) and UV for 30 min (group 2). Group 3 was only injected with UCNP-DPP-PEG in the dark as control. Group 4 was irradiated with a 980 nm laser for 30 min (2.5 W/cm^{-2}, 5 min break after 5 min irradiation). Group 5 only received saline as control. All the groups received only one nanoparticle injection. The body weights and tumor volumes were monitored every day after treatment. The tumor volume was calculated using the following equation: tumor volume (V) = length × width^2/2. Relative tumor volume was calculated as V/V_0 (V_0 was the corresponding tumor volume when the treatment was initiated).

Biodistribution of Nanoparticles in Mice. Female Balb/c mice weighing about 18−20 g were injected with UCNP-DPP-PEG nanoparticles (26 mg Gd/kg) intravenously. The mice (n = 4) were then euthanized at different time points (10 min, 1 h, 3 h, 12 h, 1 day, 3 days, and 7 days). Major organs (heart, liver, spleen, lung, and kidney) were collected and weighed. Then all the tissues were treated with HNO_3 and H_2O_2 (v/v = 1:2) at 70 °C to obtain clear solutions. The gadolinium concentrations in the solutions were determined by ICP-MS, and the contents in each tissue were calculated.

In Vivo and Ex Vivo UCL Imaging. In vivo and ex vivo UCL imaging was performed on an in vivo imaging system with an adjustable 980 nm laser as the excited source. UCL signals were corrected at 800 ± 12 nm by Andor DU897 EMCCD and analyzed with Kodak Molecular Imaging software. Before imaging, the Balb/c mice were anesthetized with 10% chloral hydrate by intraperitoneal injection. The Balb/c mice were not shaved. For intratumoral injection, UCNP-DPP-PEG nanoparticles (50 μL, 0.5 mg/mL) were injected into the tumor site of mice. For intravenous injection, UCNP-DPP-PEG nanoparticles (200 μL, 0.5 mg/mL) were injected. The UCL imaging experiments were performed at timed intervals. After 3 h, the major internal organs were removed for ex vivo imaging.

In Vitro and In Vivo T_1-Weighted MR Imaging. The in vitro MR imaging experiments were performed in a 0.5 T MRI magnet (Shanghai Niumai Corporation Ration NM120-Analyst). UCNP-DPP-PEG samples were dispersed in water at various Gd concentrations (by ICP-MS measurement). T_1 was acquired using an inversion recovery sequence. T_1 measurements were performed using a nonlinear fit to changes in the mean signal intensity within each well as a function of repetition time (TR) with a Huantong 1.5 T MR scanner. Finally, the r_1 relaxivity values were determined through the curve fitting of $1/T_1$ relaxation time (s^{-1}) versus the Gd concentration (mM).

In vivo MR imaging experiments were performed on a 1.5 T clinical MRI instrument (Siemens Medical System). The tumor-bearing mouse was anesthetized with 10% chloral hydrate by intraperitoneal injection. The mouse was scanned before and after intratumoral injection of UCNP-DPP-PEG nanoparticles (50 μL, 15 mM).

In Vitro and In Vivo X-ray CT Imaging. The in vitro CT imaging experiments were performed at 120 kVp voltages on a Philips 256-slice CT scanner (Philips Medical System). The UCNP-DPP-PEG nanoparticles and iobitridol were dispersed in PBS with various concentrations and then placed in a series of 1.5 mL tubes for CT imaging.

To perform in vivo CT imaging, the Balb/c mice were first anesthetized with 10% chloral hydrate by intraperitoneal injection. UCNP-DPP-PEG nanoparticles (50 μL, 20 mg/mL) were intratumorally injected into the tumor-bearing mouse in situ. The mouse was scanned before and after intratumoral injection. For intravenous

dx.doi.org/10.1021/ja410028q | J. Am. Chem. Soc. 2013, 135, 18920−18929

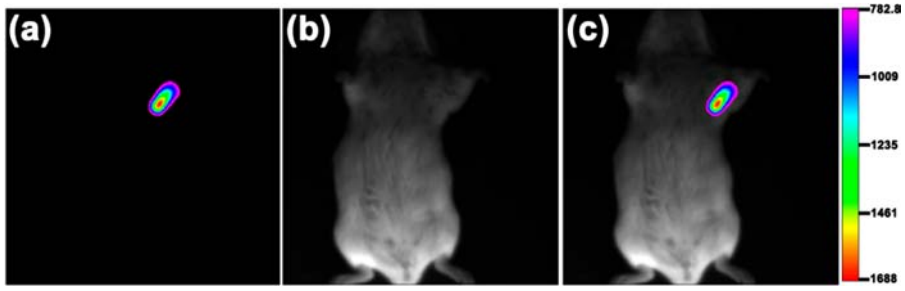

Figure 2. In vivo UCL imaging of a tumor-bearing Balb/c mouse after injection of nanoparticles at the tumor site: upconversion luminescence (a), bright field (b), and overlay images (c).

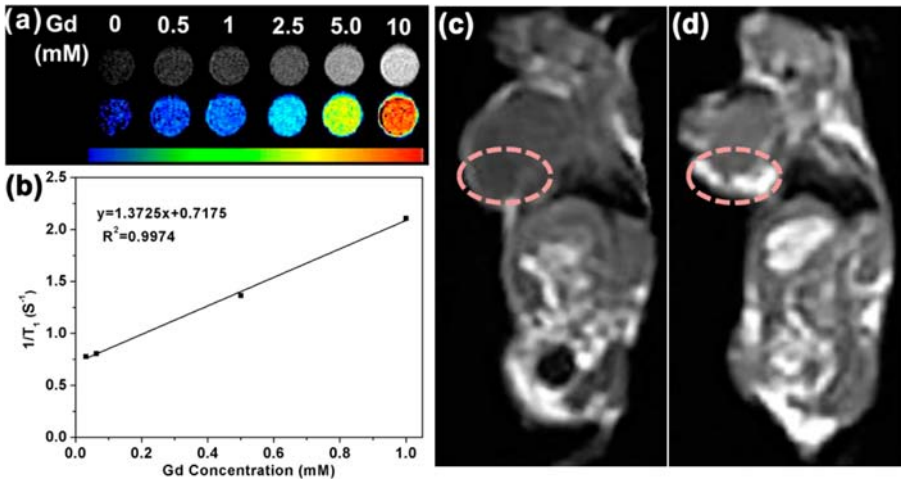

Figure 3. In vitro T_1-weighted MR images of UCNP-DPP-PEG at different Gd concentrations (a). Relaxation rate R_1 versus different molar concentrations of UCNP-DPP-PEG nanoparticles (b). T_1-weighted MR images of a tumor-bearing Balb/c mouse: preinjection (c) and after injection (d) in situ.

injection, 200 μL of UCNP-DPP-PEG nanoparticles (50 mg/mL) or iobitridol (100 mg I/mL) was injected into two mice, respectively. CT images were acquired at timed intervals. The in vivo CT imaging was performed on a Philips 256-slice CT scanner (Philips Medical System). Imaging parameters were given as follows: thickness, 0.9 mm; pitch, 0.99; 120 kVp, 300 mA; field of view, 350 mm; gantry rotation time, 0.5 s; table speed, 158.9 mm s^{-1}. Thin-section axial images were re-formed to coronal images by a computational technique referred to as multiplanar reconstruction.

RESULTS

Synthesis and Characterization of UCNP-DPP-PEG. The preparation details of DPP are described in the Supporting Information and have been verified by FTIR (Figure S1 in the Supporting Information). First, the $NaYF_4$:Yb^{3+}/Tm^{3+} core was obtained by a thermal decomposition method. Then, the active shell $NaGdF_4$:Yb^{3+} was coated on the surface through a seed-mediated process. As given in Figure 1b,c by transmission electron micrographs (TEM), the UCNPs have uniform morphology and good monodispersity with a size around 65 nm. XRD was utilized to confirm the structure of the nanoparticles (Figure S2), and the pattern of the core is consistent with the hexagonal phase structure of $NaYF_4$. After growth of the $NaGdF_4$ shell, the diffraction peaks approach the values for the $NaGdF_4$ crystal, and the relative upconversion luminescence intensity was enhanced remarkably (Figure S3). Then the core−shell structured UCNPs were transferred from nonpolar solvent to water by using polyethylenimine (PEI) as functional ligands. Dicarboxyl pro-drug DPP can conjugate with the free amine of PEI using the EDC/NHS method. We also modify the UCNP surface with PEG to gain UCNP-DPP-PEG nanoparticles to reduce the immunogenicity and antigenicity from the host's immune system.[15] Even though UCNPs were transferred from nonpolar solvent to water, UCNP-DPP-PEG still shows excellent dispersity (Figure 1c,d). We further utilized high-angle annular dark-field scanning transmission electron microscopy (HAADF-STEM) and the line profiles of the corresponding compositions to analyze the element distribution of the nanoparticles (Figure S4). The results show that Y and Gd elements are distributed in the core and shell, respectively. Pt is well-distributed on the surface of nanoparticles due to the successful conjugation of platinum(IV) pro-drug. The actual platinum content in the nanoparticles is calculated to be 26 μg of platinum/UCNP-DPP-PEG mg by ICP-MS.

UCL/MR/CT Trimodal Imaging of Nanoparticles. Compared with other optical imaging technology, UCL converts the low-energy photons (NIR) into high-energy photons (UV, visible, or NIR) via the multiphoton processes.[16] Meanwhile, UCL exhibits unique properties, such as large Stokes shift, higher penetration depth, sharp emission lines, and superior photostability. Tm^{3+}-doped UCNPs can not only emit UV and blue light but also emit NIR light at 800 nm under 980 nm laser excitation (Figure S5). Therefore, the emission at 800 nm can be used as the output signal to realize the NIR-to-NIR UCL imaging. A solution of UCNP-DPP-PEG was intratumorally injected into the tumor site on the left axilla. As given in Figure 2a−c, the bright field of mice and overlays of UCL images confirmed that a significant signal could be observed

dx.doi.org/10.1021/ja410028q | J. Am. Chem. Soc. 2013, 135, 18920−18929

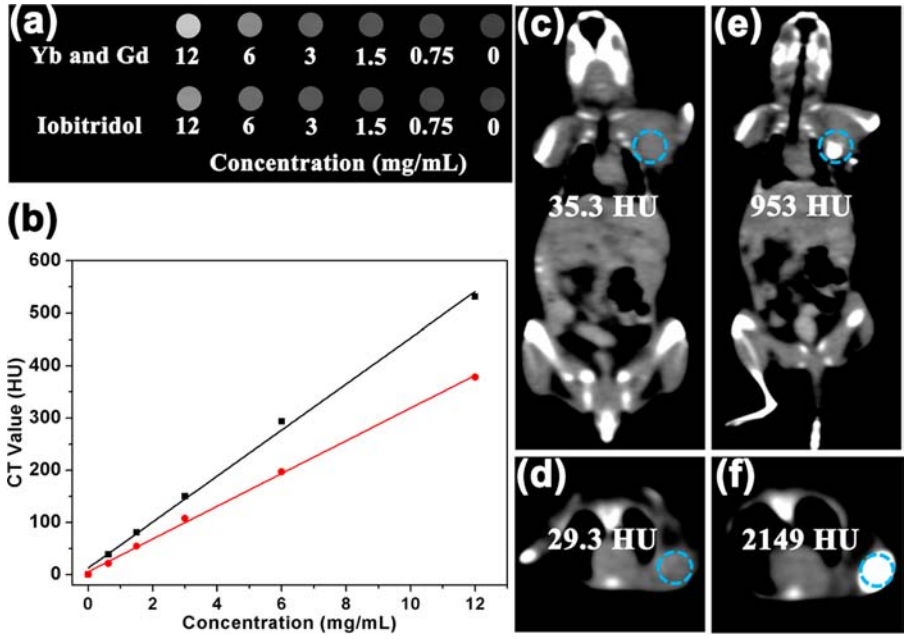

Figure 4. (a) In vitro CT images of UCNP-DPP-PEG and iobitridol at different concentrations. (b) HU value of aqueous solution of UCNP-DPP-PEG nanoparticles (black dots) and iobitridol (red dots) as a function of the concentration. (c) CT imagings of a tumor-bearing Balb/c mouse: preinjection (c,d) and after injection (e,f) in situ.

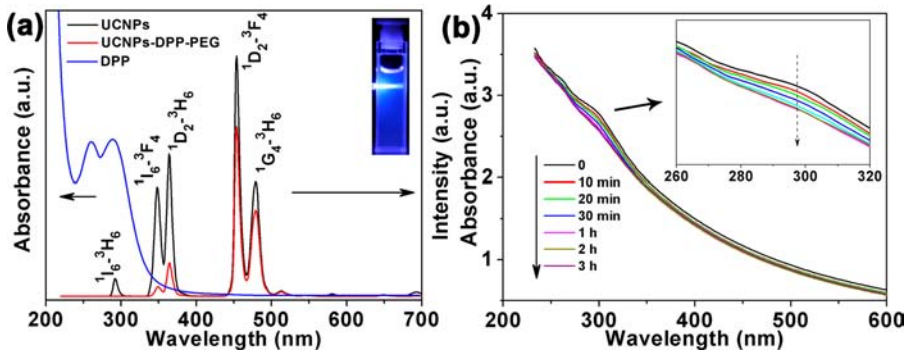

Figure 5. (a) Absorption spectrum of the DPP (blue line), emission spectra of pure UCNPs (black line), and DPP-conjugated UCNPs (red line) under 980 nm laser. (b) Absorption spectra of the UCNP-DPP-PEG as a function of time under 980 nm laser irradiation. The luminescence photograph of UCNPs under 980 nm laser in the dark is given in the inset.

from the tumor site. We also investigated the distribution of the nanoparticles by tail vein injection at timed intervals (Figure S6). The images showed a persistently strong signal in the liver. Even though the NIR-to-NIR upconversion luminescence imaging possesses higher sensitivity and deeper tissue penetration compared with traditional optical imaging, the ex vivo UCL imaging was also used to investigate the distribution of UCNP-DPP-PEG in detail. The nanoparticles accumulate in the liver, lung, and spleen after 3 h from the UCL signal ex vivo. The above results indicated that the injected UCNP-DPP-PEG could be an effective bioprobe for UCL imaging.

Due to the positive signal enhancement ability of Gd^{3+} ions, the UCNPs can be used as T_1 MRI contrast agents. As given in Figure 3a, the signals are positively enhanced at increased Gd concentration from 0 to 10 mM. The longitudinal relaxivity (R_1) values of nanoparticles are 1.3725 mM^{-1} s^{-1} (Figure 3b). We further performed in vivo MR imaging in a tumor-bearing mouse with a 1.5 T MR human clinical scanner. The solution of the nanoparticles was intratumorally injected to the mouse. As illustrated in Figure 3c,d, the tumor site shows much higher MRI signal intensity after injection, indicating that the UCNP-DPP-PEG could be used as a potential contrast agent for T_1 MR imaging.

X-ray CT is an important diagnostic imaging technique due to its high resolution and deep tissue penetration. Yb- and Gd-based/doped nanoparticles can be used as contrast agents for CT imaging.[3] Therefore, we assess CT contrast efficacy of UCNP-DPP-PEG. As shown in Figure 4a, the CT values and signals increased with increasing concentration of the nanoparticles. Compared with the commercial iobitridol at the same concentration, the nanoparticles showed higher positive contrast enhancement due to the appropriate K-edge located with the clinical X-ray spectrum.[3] In vivo CT imaging was further investigated by intratumorally injecting the solution of nanoparticles. The CT values in the tumor were up to 953 Hounsfield units (HU) and 2149 HU at coronal and transversal position, respectively. The nanoparticles were also injected intravenously into the mouse to track the distribution of nanoparticles by CT imaging. The gradual enhancement of signals for liver could be observed with time from 5 min to 2 h

dx.doi.org/10.1021/ja410028q | J. Am. Chem. Soc. 2013, 135, 18920−18929

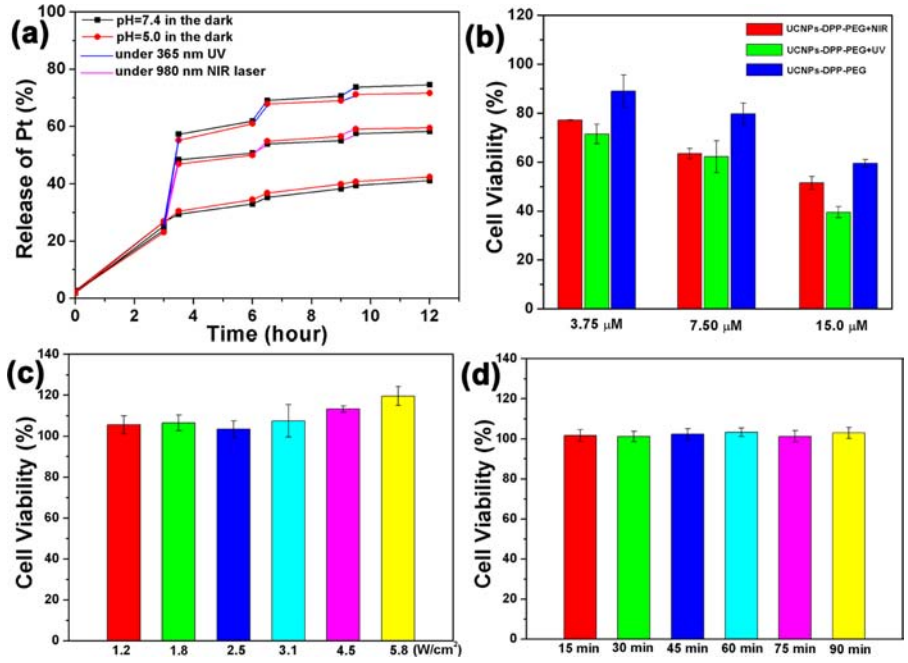

Figure 6. (a) Release profile of UCNP-DPP-PEG nanoparticles under different pH values (7.4 and 5.0) alternately changing the illumination conditions between 980 nm NIR irradiation (or 365 nm UV) and in the dark conditions. (b) In vitro HeLa cells' relative viabilities after incubation for 48 h with UCNP-DPP-PEG at different platinum concentrations. (c) Cell viability after being irradiated with 980 nm laser under different intensities for 60 min (5 min break after 5 min irradiation). (d) Cell viability after being irradiated with UV light under different irradiation times. Error bars indicate standard deviations, $N = 4$.

(Figure S7). For comparison, the iobitridol was injected to a different mouse by tail vein under the same CT protocol. The iobitridol accumulates in the kidney and then in the bladder within 30 min (Figure S8). The long circulation of nanoparticles can improve biomedical diagnosis and therapy, such as hepatic metastases and angiography.[17] The above in vitro and in vivo CT imaging studies confirm that the UCNP-DPP-PEG could be applied as a contrast agent for CT imaging.

In Vitro Control Release and Cellular Cytotoxicity Assays under 980 nm Laser Irradiation. First, whether the upconverted UV emission from UCNPs can activate the platinum(IV) pro-drug DPP should be confirmed. The upconversion emission spectra of neat UCNPs and UCNP-DPP together with absorption spectrum of DPP are given in Figure 5a. Obviously, the absorption spectrum of DPP overlaps the UV emission of UCNPs at 291 nm ($^1I_6$-$^3H_6$), 346 nm ($^1I_6$-$^3F_4$), and 363 nm ($^1D_2$-$^3H_6$). After conjugation of DPP on the surface of UCNPs, the upconversion emission at the UV part decreases sharply. Furthermore, the emission intensity of UCNP-DPP at 452 and 477 nm becomes weaker than that of the neat UCNPs. The blue emission of the UCNPs may also activate DPP, which has low absorbance in the visible region.[11a] The above results confirm the energy transfer process between UCNPs and DPP. Even though the maximum absorbance of DPP (289 nm) is not matched precisely with the emission of UCNPs (365 nm), it is confirmed that the 365 nm UV can also effectively activate the platinum(IV) pro-drug, as shown in Figure S9. This is in agreement with a previous report.[11a] In order to determine whether the pro-drug DPP can be activated by NIR or not, the absorption spectra of the UCNP-DPP-PEG as a function exposure time by 980 nm NIR irradiation are shown in Figure 5b. The absorption spectra of UCNP-DPP-PEG decrease in intensity at 289 nm with increasing NIR irradiation time, which indicates loss of platinum−azide bonds in the DPP structure.[11] We also do the parallel experiment under 365 nm UV irradiation (Figure S10). Both absorption spectra under NIR and UV irradiation showed a similar shift in the trend. Therefore, the 980 nm laser irradiation can effectively activate the platinum(IV) pro-drug.

The photoinduced drug-controlled release process from UCNP-DPP-PEG at different pH values was investigated. The contents of platinum were determined accurately by ICP-MS. Figure 6a gives the drug release profiles of UCNP-DPP-PEG at different pH values (7.4 and 5.0) of PBS buffer solution by alternately changing the illumination conditions between 980 nm NIR irradiation (or 365 nm UV) and in the dark conditions. First, the solutions of the nanoparticles were placed at 37 °C in the dark for 4 h, and about 25% of platinum was released, which may be attributed to the hydrolysis reaction of ester linkages between the UCNPs and platinum(IV) complexes.[18] Meanwhile, we found that the pH values (7.4 and 5.0) did not affect the release process of the platinum drug. After that, the nanoparticles were exposed to 980 nm NIR light (or 365 nm UV) for only 30 min, and the platinum release amount reached 48.4% (57.3% under UV) at pH 7.4. In contrast, only a small amount of platinum was released from the nanoparticles in the dark. The stability of UCNP-DPP-PEG in serum was also tested in the dark by ICP-MS. The pro-drugs were released in a slow fashion, and only 30% of pro-drugs were released after 48 h in the dark (Figure S11). This result suggests that these UCNP-DPP-PEG nanoparticles also possess good stability in blood circulation. According to the absorption spectra under NIR and UV irradiation, rough calculations were made to find that the DPP molecules released per particle were around 3000 and 10 000 after 1 h irradiation under 980 nm laser and 365 nm UV light irradiation, respectively (detailed calculations are given in Supporting Information). Thus thousands of drug molecules are released per nanoparticle

dx.doi.org/10.1021/ja410028q | J. Am. Chem. Soc. 2013, 135, 18920−18929

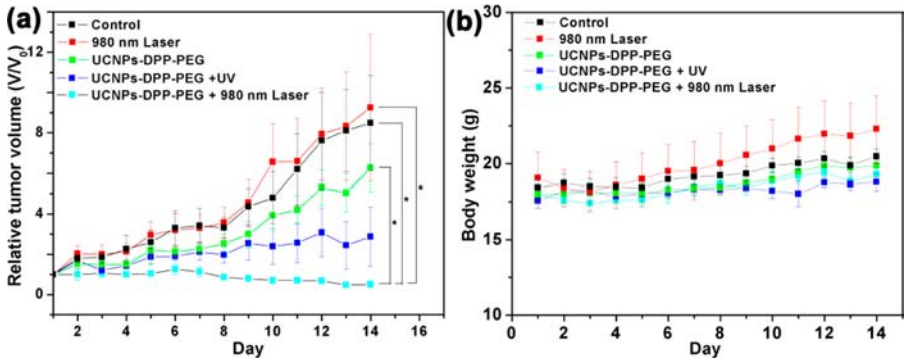

Figure 7. In vivo tumor volume changes of Balb/c mice on different groups after various treatments, 980 nm laser irradiation for 30 min (2.5 W/cm^{-2}, 5 min break after 5 min irradiation), UV (365 nm) irradiation for 30 min, or without any irradiation (a); the relative tumor volumes were normalized to their initial volumes before the treatment; *P < 0.05. Body weight changes with time of Balb/c mice under different treatments (b). Error bars indicate standard deviations; N = 6.

under 980 nm laser or UV light irradiation. The 980 nm NIR light (or 365 nm UV) can enhance the drug release effectively because the platinum(IV) pro-drug DPP has been activated and changed to platinum(II) complexes under the irradiation of upconverted UV emission from UCNPs (or UV directly). Therefore, the UCNPs can not only release the drug from the nanoparticles under 980 nm NIR irradiation but also activate the pro-drug to gain a high toxicity platinum(II) drug to kill the cancer cells at the same time.

To further investigate whether the platinum(II) complexes from *trans*-platinum(IV) pro-drug DPP-conjugated UCNPs are pharmacologically active or not under NIR excitation, MTT protocol was carried out to evaluate the cytotoxic effect of UCNP-DPP-PEG against cancer cells under 980 nm NIR irradiation. HeLa cells with the UCNP-DPP-PEG irradiated under UV and the HeLa cells only with the UCNP-DPP-PEG were used as a control under the same condition. First, UCNP-DPP-PEG nanoparticles were incubated with HeLa cells for 4 h to internalize the nanoparticles. Then the cells were exposed to a 980 nm laser (4.5 W/cm^2, 5 min break after 5 min irradiation) or UV irradiation for 40 min. After that, the cells were further incubated in the dark for 48 h. The cell viability of HeLa cells under different conditions is given in Figure 6b. Although the cell viabilities decrease gradually with the increase of the concentration of the sample in the dark, the UCNP-DPP-PEG nanoparticles exhibited better inhibition against HeLa cells under UV or 980 nm laser. The phototoxicity of the 980 nm laser and UV light was also investigated in detail. It is shown that the 980 nm laser irradiation does not lower the cell viability under different irradiation intensity, as given in Figure 6c. The 980 nm laser irradiation can increase the water temperature, but the short interval irradiation could avoid the overheating of the culture medium. Thus, the 980 nm laser irradiation is safe for the cells. Excessive exposure to UV irradiation could damage the cells. Therefore, the cytotoxic effect of UV irradiation under different irradiation time is given in Figure 6d. We could find that UV light did not affect the cell growth after 90 min irradiation. UV light within 90 min irradiation is also safe for the cells. The above results indicate that the 980 nm laser only or UV light only has no toxic effects on the cells. Thus, the platinum(IV) pro-drugs can be activated under UV or 980 nm laser by the NIR-to-UV strategy to kill cancer cells. In addition, ICP-MS was used to determine the platinum content in the cells. As shown in Figure S12, the mass of platinum internalized in HeLa cells from UCNP-DPP-PEG nanoparticles was much higher than that of the free DPP after being incubated for the same time. We also used upconversion fluorescence imaging of UCNPs to determine the location of nanoparticles in the cells (Figure S13). As the incubation time was prolonged to 3 h, more and more nanoparticles were internalized into the cells. Thus the UCNPs can effectively deliver the platinum(IV) pro-drugs into the cells. Hence, more platinum(IV) pro-drugs can be activated by upconverted UV emission under 980 nm NIR laser irradiation to form more cytotoxic platinum(II) complexes to kill the cancer cells.

In Vivo Tumor Inhibition Ability of Nanoparticles under 980 nm Laser Irradiation. Further experiments were conducted to evaluate the tumor inhibition efficacy of the UCNP-DPP-PEG under 980 nm laser irradiation in vivo. The liver cancer tumor cell line H22 (murine hepatocarcinoma) was selected as the xenograft model. The tumor-bearing Balb/c mice were divided into five groups (n = 6) randomly. We intratumorally injected the UCNP-DPP-PEG in the first three groups. After 4 h, the tumor site was irradiated with 980 nm laser for 30 min (2.5 W/cm^{-2}, 5 min break after 5 min irradiation, as given in Figure S14, group 1) and UV for 30 min (group 2). Group 3 was only injected with UCNP-DPP-PEG in the dark as the control. The injected Pt (conjugated nanoparticles) dose in 80 μL of saline was 0.65 mg/kg body weight. Similar to group 1, group 4 was exposed to the 980 nm laser for 30 min without injection of UCNP-DPP-PEG. Group 5 was only intratumorally injected with saline (80 μL) as the control. We injected the nanoparticles and irradiated therapy to the tumor site only one time. As shown in Figure 7a, the group treated with UCNP-DPP-PEG + 980 nm laser irradiation demonstrated the best tumor growth inhibition efficacy. The digital photos of representative mice with excised tumors (Figure S15) also showed that the tumor sizes under UCNP-DPP-PEG + 980 nm laser irradiation treatments were smaller than the those of other groups. The pure 980 nm laser irradiation (group 4) showed no obvious effect on the tumor size. We also designed the experiment to test the surface temperature of the tumor site before and after the 980 nm laser irradiation at a power density of 2.5 W/cm^2 by an infrared thermometer. The surface temperature of the skin at the tumor site is about 27.1 °C (four parallel experiments) before the irradiation, and the laboratory temperature is 12 °C. After 5 min irradiation by the 980 nm laser, the surface temperature of the skin at the tumor site increased to about 31.0 °C. However, the surface temperature reduced to 27.6 °C after the 980 nm

dx.doi.org/10.1021/ja410028q | J. Am. Chem. Soc. 2013, 135, 18920−18929

laser was shut down for 5 min. Meanwhile, the surface of the skin at the site of irradiation did not have any scars caused by 980 nm laser irradiation. This can be attributed to the fact that the NIR light is safe for the tissue and short interval irradiation can avoid overheating by the NIR light. Moreover, the group under UCNP-DPP-PEG + 980 nm laser irradiation exhibited better tumor inhibition than that under UCNP-DPP-PEG + UV (365 nm) irradiation, which could be attributed to the deeper tissue penetration of NIR light than UV light. Even though the xenograft tumor is just under the surface of the skin, the UV still cannot penetrate the skin effectively to activate the pro-drug. Therefore, the NIR-to-UV approach is more practical in the biomedical field. In addition, the representative photographs of mice from different groups on the 15th day, and hematoxylin and eosin (H&E) staining images of tumor sections are given in Figure S16. Most tumor tissue cells under UCNP-DPP-PEG + 980 nm laser irradiation were destroyed compared to the others. Body weight is an important parameter to evaluate the systemic toxicity of the material to the body. As given in Figure 7b, the body weight of all groups does not decrease with the time prolonged, indicating that the pro-drugs-conjugated UCNPs could reduce the adverse side effects of traditional anticancer drugs. In addition, ICP-MS was used to determine in vivo long-term tissue biodistribution of UCNP-DPP-PEG nanoparticles in mice. As given in Figure S17, in the early stages after the injection, the nanoparticles accumulated in the lungs. As time was extended, high concentrations of Gd were observed in liver, spleen, and lung by 1 h post-injection of nanoparticles. The concentrations of nanoparticles are very low in heart and kidney at all time points after post-injection. Nanoparticles accumulate in the spleen within 24 h post-injection, which may be the reason why the spleen is the largest organ of the immune system. After 24 h post-injection, the concentrations of nanoparticles reduced in liver, spleen, and lung. By day 7, the nanoparticles in the liver, spleen, and lung were much less than the first 24 h after the injection. From the changes of nanoparticles in the organs, the nanoparticles could generally be excreted from the mice as time prolonged.

DISCUSSION

In this study, we develop a multifunctional nanomedicine system which combines cancer diagnosis and therapy together. Lanthanide-doped UCNPs not only can be used as drug delivery host carrier but also can be applied as contrast agents for UCL/MR/CT trimodality imaging. Most importantly in this study, the UCNPs are used as nanotransducers by converting deeply penetrating NIR light into UV to activate the platinum pro-drug. High-energy UV can achieve many photoreactions or changes in the molecular structure, which may result in a large variety of applications in the field of nanomedicine, as the UV radiation can induce gene mutations to the normal tissue cells and have poor tissue penetration depth, which limits its practical application.[19] Therefore, we demonstrate a NIR-to-UV strategy by utilizing 980 nm NIR laser excited UCNPs as the indirect UV source. The 980 nm NIR light is safer for health and has tissue penetration as deep as 3.2 cm according to previous reports, which is suitable for practical bioapplications.[6c] The Yb^{3+}/Tm^{3+}-co-doped $NaYF_4$ nanoparticles can emit phonons in the UV regions (from 290 to 370 nm). Yb^{3+}-doped $NaGdF_4$ active shell has been coated around $NaYF_4$:Yb^{3+}/Tm^{3+} to enhance the luminescent intensity. In addition, the Gd^{3+} in the shell can also serve as an MRI contrast agent.[2a] The UCNPs can also emit 800 nm NIR light under 980 nm excitation, which is suitable for UCL imaging.[2c] Yb- and Gd-based/doped nanoparticles can be used as contrast agents for CT imaging.[3] In the study, the UCL/MR/CT trimodality imaging has been combined into one nanomedical system, which integrates the advantages of different imaging modality techniques together to avoid the shortcomings of single imaging modality. Therefore, the multimodality imaging of nanoparticles can enhance the efficiency and accuracy for diagnosis. On the other hand, the platinum(IV) pro-drug DPP has been successfully synthesized and conjugated on the surface of the UCNPs directly. Compared with the physical adsorption, the covalent bond conjugation can prevent drug release before reaching the tumor site. Hence, this drug delivery system can reduce the pro-drug release in the blood circulation and release the platinum drug to kill the cancer cells at the tumor site. Additionally, the nanoparticles may leak a small amount of pro-drug before arriving at the targeted location by hydrolysis reaction of ester linkages between the UCNPs and platinum(IV) complexes, but the platinum(IV) pro-drug has little toxicity to health and is excreted out quickly. This nanomedical platform can reduce the toxic side effects of chemotherapeutic drugs and enhanced therapeutic efficacy.

First, experiments were performed to certify the basic principle that the *trans*-platinum(IV) pro-drug could be activated by NIR irradiation through the NIR-to-UV approach. The DPP lost the platinum−azide bonds and were reduced to platinum(II) drugs under UV light irradiation. The absorbance intensity of DPP decreased with prolonged 980 nm NIR irradiation time, which has a similar shift trend to that under 365 nm UV directly. Most importantly, the UCNPs activate the pro-drug to high toxicity platinum(II) drug, which was released from UCNPs at the same time. Then we evaluate in vitro cytotoxicity of UCNP-DPP-PEG under 980 nm laser irradiation. The UCNP-DPP-PEG nanoparticles exhibited significantly enhanced inhibition against HeLa cells under 980 nm laser irradiation due to the photoactivated DPP to kill cancer cells. It is worth mentioning that the small molecules like cisplatin or DPP can be diffused into cells whereas the nanoparticles have to be endocytosed to enter the cells.[20] The mass of platinum internalized in HeLa cells from UCNP-DPP-PEG (5.694 pg/cell) was much higher than the free DPP (0.35 pg/cell) after being incubated for 6 h. Thus the UCNPs can effectively deliver the platinum(IV) pro-drugs into the cells. Moreover, further in vivo experiments revealed that UCNP-DPP-PEG under 980 nm laser and UV (365 nm) irradiation can suppress the tumor growth. Interestingly, the pro-drug-conjugated UCNPs under 980 nm laser exhibited more efficacy than the one under UV in vivo. In fact, the upconversion quantum yield is lower than 0.3%,[21] thus the intensity of upconverted UV emission is much lower than the direct UV irradiation. However, the group with UCNP-DPP-PEG under 980 nm NIR irradiation demonstrated better inhibition of tumor growth than under direct UV irradiation due to the higher tissue penetration depth of NIR light. In addition, we injected the nanoparticles and irradiated therapy to the tumor site only one time. The nanoparticles can effectively suppress tumor growth under 980 nm laser irradiation. Compared with the traditional multiple dosing of anticancer drugs, this nanomedical platform is more efficient in biomedical applications.

The photodynamic therapy (PDT) is an alternative treatment strategy in cancer treatment. However, PDT requires a

photosensitizer, light, and oxygen that are combined together to kill cancer cells.[13e,22] Unfortunately, the hypoxic condition of most tumor tissues limits the clinical applications of PDT. In this study, the photoactivated pro-drug does not require the oxygen molecule. Therefore, the photoactivation *trans*-platinum(IV) pro-drug has a more promising application in cancer therapy. In addition, the mechanism of photoactivated *trans*-platinum(IV) pro-drug to kill the cancer cells after UV irradiation is not completely well-understood so far. Sadler's group has reported the light-activated platinum(IV) pro-drug *trans,trans,trans*-$[Pt(N_3)_2(NH_3)(py)(OH)_2]$ for the first time.[11a] They believe that the photoactivated pro-drug forms *trans* G adducts both with model G derivatives and with plasmid DNA, and the mechanism is different from cisplatin.[11a] After that, Bednarski and Sadler further did research on this pro-drug, and they found that $[Pt(OH)_2NH_3(py)]$ was gained after UV irradiation, and autophagy might be active during cell death.[23] Even though the mechanism is not understood completely, the pro-drug that can express toxicity to kill cancer cells under UV irradiation has been confirmed. The aim of the present work was to utilize the photoactivated pro-drug to realize the tumor exhibition through NIR-to-UV strategy. The in vivo experiments showed better antitumor effect than in vitro experiments, and some factors may affect the results between in vitro and in vivo experiments. The treatment time and the doses of pro-drugs are different between in vitro and in vivo experiments. It should be noted that we choose intratumoral injection of UCNP-DPP-PEG to prove the concept of our approach. Compared with the intravenous injection, the injection of nanoparticles in situ can enrich the nanoparticles in the tumor sites to achieve better tumor exhibition. Indeed, the intravenous injection is more practical in the clinical treatment, and further studies by intravenous injection of tumor-targeting nanoparticles are currently in progress in our group.

CONCLUSION

The present work is the first example of using UCNPs as nanotransducers by converting deeply penetrating NIR light into UV to control the anticancer drug activity together with trimodality imaging. The UCNP-DPP-PEG entering the cell via endocytosis can ensure that a large number of pro-drugs were brought into the cells. Hence, the UCNP-DPP-PEG can effectively kill cancer cells under 980 nm laser irradiation. Importantly, the mice treated with UCNP-DPP-PEG under 980 nm laser demonstrated better tumor growth inhibition efficacy than that under 365 nm UV irradiation. In addition, the UCNPs can be used as contrast agents for UCL/MR/CT trimodality imaging, which could provide complete information to guide the cancer treatment. Our findings suggest that using the NIR-to-UV approach is more effective in practical cancer therapy than using the UV directly due to the higher tissue penetration depth of NIR light. Therefore, this multifunctional hybrid system not only can be utilized as the contrast agents for image-guided therapy but also can serve as a transducer to utilize upconverted UV emission under NIR irradiation to treat cancer in a practical therapy process.

ASSOCIATED CONTENT

Supporting Information

The preparation details of DPP, the rough calculation process of the number of DPP molecules released from per nanoparticles, and Figures S1−S17. This material is available free of charge via the Internet at http://pubs.acs.org.

AUTHOR INFORMATION

Corresponding Authors

mapa675@ciac.ac.cn (P.M.)
yangpiaoping@hrbeu.edu.cn (P.Y.)
jlin@ciac.ac.cn (J.L.)

Notes

The authors declare no competing financial interest.

ACKNOWLEDGMENTS

This project is financially supported by the National Natural Science Foundation of China (NSFC 51332008, 51372241, 21221061) and the National Basic Research Program of China (2014CB643803). We thank Prof. Fuyou Li and Min Chen from Fudan University for performing the upconversion fluorescent imaging experiments of mice in vivo.

REFERENCES

(1) (a) Brigger, I.; Dubernet, C.; Couvreur, P. *Adv. Drug Delivery Rev.* **2002**, *54*, 631. (b) Peer, D.; Karp, J. M.; Hong, S.; Farokhzad, O. C.; Margalit, R.; Langer, R. *Nat. Nanotechnol.* **2007**, *2*, 751. (c) Chen, H.; Zhen, Z.; Todd, T.; Chu, P. K.; Xie, J. *Mater. Sci. Eng. Res.* **2013**, *74*, 35. (d) Doane, T. L.; Burda, C. *Chem. Soc. Rev.* **2012**, *41*, 2885. (e) Such, G. K.; Johnston, A. P. R.; Caruso, F. *Chem. Soc. Rev.* **2011**, *40*, 19.

(2) (a) Lee, N.; Choi, S. H.; Hyeon, T. *Adv. Mater.* **2013**, *25*, 2641. (b) Gu, Z.; Yan, L.; Tian, G.; Li, S.; Chai, Z.; Zhao, Y. *Adv. Mater.* **2013**, *25*, 3758. (c) Zhou, J.; Liu, Z.; Li, F. Y. *Chem. Soc. Rev.* **2012**, *41*, 1323. (d) Bigall, N. C.; Parak, W. J.; Dorfs, D. *Nano Today* **2012**, *7*, 282.

(3) (a) Liu, Y. L.; Ai, K. L.; Liu, J. H.; Yuan, Q. H.; He, Y. Y.; Lu, L. H. *Angew. Chem., Int. Ed.* **2012**, *51*, 1437. (b) Li, F. F.; Li, C. G.; Liu, J. H.; Liu, X. M.; Zhao, L.; Bai, T. Y.; Yuan, Q. H.; Kong, X. G.; Han, Y.; Shi, Z.; Feng, S. H. *Nanoscale* **2013**, *5*, 6950.

(4) Viswanathan, S.; Kovacs, Z.; Green, K. N.; Ratnakar, S. J.; Sherry, A. D. *Chem. Rev.* **2010**, *110*, 2960.

(5) (a) Wang, F.; Han, Y.; Lim, C. S.; Lu, Y. H.; Wang, J.; Xu, J.; Chen, H. Y.; Zhang, C.; Hong, M. H.; Liu, X. G. *Nature* **2010**, *463*, 1061. (b) Cheng, L.; Yang, K.; Li, Y.; Chen, J.; Wang, C.; Shao, M.; Lee, S.-T.; Liu, Z. *Angew. Chem., Int. Ed.* **2011**, *50*, 7385. (c) Zhao, J.; Jin, D.; Schartner, E. P.; Lu, Y.; Liu, Y.; Zvyagin, A. V.; Zhang, L.; Dawes, J. M.; Xi, P.; Piper, J. A.; Goldys, E. M.; Monro, T. M. *Nat. Nanotechnol.* **2013**, *8*, 729. (d) Mader, H. S.; Kele, P.; Saleh, S. M.; Wolfbeis, O. S. *Curr. Opin. Chem. Biol.* **2010**, *14*, 582. (e) Fan, W.; Shen, B.; Bu, W.; Chen, F.; Zhao, K.; Zhang, S.; Zhou, L.; Peng, W.; Xiao, Q.; Xing, H.; Liu, J.; Ni, D.; He, Q.; Shi, J. *J. Am. Chem. Soc.* **2013**, *135*, 6494. (f) Liu, Y.; Tu, D.; Zhu, H.; Chen, X. *Chem. Soc. Rev.* **2013**, *42*, 6924. (g) Kar, A.; Patra, A. *Nanoscale* **2012**, *4*, 3608. (h) Bunzli, J.-C. G.; Eliseeva, S. V. *Chem. Sci.* **2013**, *4*, 1939. (i) Wang, G.; Peng, Q.; Li, Y. *Acc. Chem. Res.* **2011**, *44*, 322. (j) Shen, J.; Zhao, L.; Han, G. *Adv. Drug Delivery Rev.* **2013**, *65*, 744. (k) Wang, H.-Q.; Batentschuk, M.; Osvet, A.; Pinna, L.; Brabec, C. J. *Adv. Mater.* **2011**, *23*, 2675. (l) Guo, H.; Sun, S. *Nanoscale* **2012**, *4*, 6692. (m) Hao, S. W.; Chen, G. Y.; Yang, C. H. *Theranostics* **2013**, *3*, 331. (n) Ye, X. C.; Collins, J. E.; Kang, Y. J.; Chen, J.; Chen, D. T. N.; Yodh, A. G.; Murray, C. B. *Proc. Natl. Acad. Sci. U.S.A.* **2010**, *107*, 22430. (o) Gorris, H. H.; Wolfbeis, O. S. *Angew. Chem., Int. Ed.* **2013**, *52*, 3584. (p) Wang, H.-Q.; Nann, T. *ACS Nano* **2010**, *4*, 1768. (q) Chan, E. M.; Han, G.; Goldberg, J. D.; Gargas, D. J.; Ostrowski, A. D.; Schuck, P. J.; Cohen, B. E.; Milliron, D. J. *Nano Lett.* **2012**, *12*, 3839.

(6) (a) Haase, M.; Schäfer, H. *Angew. Chem., Int. Ed.* **2011**, *50*, 5808. (b) Zhang, F.; Che, R. C.; Li, X. M.; Yao, C.; Yang, J. P.; Shen, D. K.; Hu, P.; Li, W.; Zhao, D. Y. *Nano Lett.* **2012**, *12*, 2852. (c) Chen, G. Y.; Shen, J.; Ohulchanskyy, T. Y.; Patel, N. J.; Kutikov, A.; Li, Z. P.; Song, J.; Pandey, R. K.; Agren, H.; Prasad, P. N.; Han, G. *ACS Nano* **2012**, *6*,

8280. (d) Dai, Y.; Yang, D.; Ma, P. A.; Kang, X.; Zhang, X.; Li, C.; Hou, Z.; Cheng, Z.; Lin, J. *Biomaterials* **2012**, *33*, 8704. (e) Dong, H.; Sun, L.-D.; Yan, C.-H. *Nanoscale* **2013**, *5*, 5703. (f) Bouzigues, C.; Gacoin, T.; Alexandrou, A. *ACS Nano* **2011**, *5*, 8488. (g) Gnach, A.; Bednarkiewicz, A. *Nano Today* **2012**, *7*, 532. (h) Qiu, P.; Zhou, N.; Chen, H.; Zhang, C.; Gao, G.; Cui, D. *Nanoscale* **2013**, *5*, 11512. (i) van der Ende, B. M.; Aarts, L.; Meijerink, A. *Adv. Mater.* **2009**, *21*, 3073. (j) Paudel, H. P.; Zhong, L.; Bayat, K.; Baroughi, M. F.; Smith, S.; Lin, C.; Jiang, C.; Berry, M. T.; May, P. S. *J. Phys. Chem. C* **2011**, *115*, 19028. (k) Liu, X. M.; Zheng, M.; Kong, X. G.; Zhang, Y. L.; Zeng, Q. H.; Sun, Z. C.; Buma, W. J.; Zhang, H. *Chem. Commun.* **2013**, *49*, 3224.

(7) Zeng, S. J.; Tsang, M. K.; Chan, C. F.; Wong, K. L.; Fei, B.; Hao, J. H. *Nanoscale* **2012**, *4*, 5118.

(8) (a) Wang, X.; Guo, Z. *Chem. Soc. Rev.* **2013**, *42*, 202. (b) Kelland, L. *Nat. Rev. Cancer* **2007**, *7*, 573.

(9) Jung, Y.; Lippard, S. J. *Chem. Rev.* **2007**, *107*, 1387.

(10) Muller, P.; Schroder, B.; Parkinson, J. A.; Kratochwil, N. A.; Coxall, R. A.; Parkin, A.; Parsons, S.; Sadler, P. J. *Angew. Chem., Int. Ed.* **2003**, *42*, 335.

(11) (a) Mackay, F. S.; Woods, J. A.; Heringova, P.; Kasparkova, J.; Pizarro, A. M.; Moggach, S. A.; Parsons, S.; Brabec, V.; Sadler, P. J. *Proc. Natl. Acad. Sci. U.S.A.* **2007**, *104*, 20743. (b) Farrer, N. J.; Woods, J. A.; Salassa, L.; Zhao, Y.; Robinson, K. S.; Clarkson, G.; Mackay, F. S.; Sadler, P. J. *Angew. Chem., Int. Ed.* **2010**, *49*, 8905.

(12) Berners-Price, S. J. *Angew. Chem., Int. Ed.* **2011**, *50*, 804.

(13) (a) Yan, B.; Boyer, J. C.; Branda, N. R.; Zhao, Y. *J. Am. Chem. Soc.* **2011**, *133*, 19714. (b) Jayakumar, M. K.; Idris, N. M.; Zhang, Y. *Proc. Natl. Acad. Sci. U.S.A.* **2012**, *109*, 8483. (c) Yang, Y. M.; Shao, Q.; Deng, R. R.; Wang, C.; Teng, X.; Cheng, K.; Cheng, Z.; Huang, L.; Liu, Z.; Liu, X. G.; Xing, B. G. *Angew. Chem., Int. Ed.* **2012**, *51*, 3125. (d) Zhang, B. F.; Frigoli, M.; Angiuli, F.; Vetrone, F.; Capobianco, J. A. *Chem. Commun.* **2012**, *48*, 7244. (e) Idris, N. M.; Gnanasammandhan, M. K.; Zhang, J.; Ho, P. C.; Mahendran, R.; Zhang, Y. *Nat. Med.* **2012**, *18*, 1580. (f) Liu, J.; Bu, W.; Pan, L.; Shi, J. *Angew. Chem., Int. Ed.* **2013**, *52*, 4375. (g) Zhao, L.; Peng, J.; Huang, Q.; Li, C.; Chen, M.; Sun, Y.; Lin, Q.; Zhu, L.; Li, F. *Adv. Funct. Mater.* **2013**, DOI: 10.1002/adfm.201302133. (h) Chien, Y.-H.; Chou, Y.-L.; Wang, S.-W.; Hung, S.-T.; Liau, M.-C.; Chao, Y.-J.; Su, C.-H.; Yeh, C.-S. *ACS Nano* **2013**, *7*, 8516.

(14) Wei, Y.; Lu, F.; Zhang, X.; Chen, D. *Chem. Mater.* **2006**, *18*, 5733.

(15) Ryan, S. M.; Mantovani, G.; Wang, X. X.; Haddleton, D. M.; Brayden, D. J. *Expert Opin. Drug Delivery* **2008**, *5*, 371.

(16) (a) Liu, Y.; Chen, M.; Cao, T.; Sun, Y.; Li, C.; Liu, Q.; Yang, T.; Yao, L.; Feng, W.; Li, F. *J. Am. Chem. Soc.* **2013**, *135*, 9869. (b) Shan, G. B.; Weissleder, R.; Hilderbrand, S. A. *Theranostics* **2013**, *3*, 267. (c) Wang, M.; Abbineni, G.; Clevenger, A.; Mao, C.; Xu, S. *Nanomedicine* **2011**, *7*, 710. (d) Zhan, Q. Q.; He, S. L.; Qian, J.; Cheng, H.; Cai, F. H. *Theranostics* **2013**, *3*, 306.

(17) Kim, D.; Park, S.; Lee, J. H.; Jeong, Y. Y.; Jon, S. *J. Am. Chem. Soc.* **2007**, *129*, 7661.

(18) Xiao, H.; Qi, R.; Liu, S.; Hu, X.; Duan, T.; Zheng, Y.; Huang, Y.; Jing, X. *Biomaterials* **2011**, *32*, 7732.

(19) D'Orazio, J.; Jarrett, S.; Amaro-Ortiz, A.; Scott, T. *Int. J. Mol. Sci.* **2013**, *14*, 12222.

(20) Nel, A. E.; Madler, L.; Velegol, D.; Xia, T.; Hoek, E. M. V.; Somasundaran, P.; Klaessig, F.; Castranova, V.; Thompson, M. *Nat. Mater.* **2009**, *8*, 543.

(21) Boyer, J. C.; van Veggel, F. *Nanoscale* **2010**, *2*, 1417.

(22) (a) Brown, S. B.; Brown, E. A.; Walker, I. *Lancet Oncol.* **2004**, *5*, 497. (b) Ethirajan, M.; Chen, Y. H.; Joshi, P.; Pandey, R. K. *Chem. Soc. Rev.* **2011**, *40*, 340. (c) Wang, C.; Cheng, L.; Liu, Y.; Wang, X.; Ma, X.; Deng, Z.; Li, Y.; Liu, Z. *Adv. Funct. Mater.* **2013**, *23*, 3077. (d) Wang, C.; Tao, H.; Cheng, L.; Liu, Z. *Biomaterials* **2011**, *32*, 6145.

(23) Westendorf, A. F.; Woods, J. A.; Korpis, K.; Farrer, N. J.; Salassa, L.; Robinson, K.; Appleyard, V.; Murray, K.; Grunert, R.; Thompson, A. M.; Sadler, P. J.; Bednarski, P. J. *Mol. Cancer Ther.* **2012**, *11*, 1894.